

Dependence of magnetization reversal on the crystallite size in MnBi thin films: Experiment, theory, and computer simulation

U. Nowak

Theoretische Tieftemperaturphysik, Gerhard-Mercator-Universität Duisburg, 47048 Duisburg, Germany

U. Rüdiger, P. Fumagalli, and G. Güntherodt

2. Physikalisches Institut, RWTH Aachen, 52056 Aachen, Germany

(Received 22 February 1996; revised manuscript received 8 July 1996)

A micromagnetic model is proposed to explain the magnetization reversal of thermally evaporated MnBi thin films. The model assumes that the films consist of grains on a square lattice with perpendicular magnetic anisotropy. In order to describe the magnetic reversal of a particular grain, dipole coupling, wall energy, Zeeman energy, and an energy barrier for the reversal of a single grain are taken into account. Disorder is included by random fluctuations of the lateral grain size in the Zeeman-energy term. The simulation is carried out by using a Monte Carlo method. The experimentally observed decrease in coercivity with increasing film thickness is accurately described by the model and can be explained by an increase in lateral grain size. The asymmetry of the slope of the hysteresis curve of thicker MnBi films can be understood in terms of disorder. In the presence of fluctuations in grain size, large grains reverse more easily than small ones leading to an asymmetry of the slope of the hysteresis curve. [S0163-1829(96)04842-4]

I. INTRODUCTION

The ferromagnetic system MnBi has been extensively studied over the past 40 years.¹⁻³ Being one of the first candidates for magneto-optic recording materials, MnBi has attracted a lot of interest mainly because of its extraordinarily large magneto-optic Kerr rotation. It reaches values of almost 2° through a glass substrate over a wide photon-energy range.⁴ In addition, the hexagonal NiAs structure provides the necessary uniaxial anisotropy in order to make a perpendicular recording media. However, it was soon realized that some other properties were rather detrimental for an application. First is a structural phase transition at 340–355 °C in connection with a magnetic phase transition from a ferromagnetic low-temperature phase to a paramagnetic high-temperature phase.⁵ Second is an anomaly in the temperature dependence of the coercive field leading to an increase of the coercivity up to 280 °C, which is of course disastrous for thermomagnetic recording.⁶

The purpose of our work is to study the interplay between structural, magnetic, and magneto-optic properties in thermally evaporated MnBi thin films. The films are not covered with a protective SiO_x layer in order to be able to study the topography of bare MnBi films. We review the magnetic properties of MnBi thin films and propose a micromagnetic model which explains the thickness dependence and the asymmetry of the hysteresis curves. By using a Monte Carlo method, hysteresis curves are simulated and compared to experiment.

II. EXPERIMENTAL METHODS

Bi/Mn multilayers have been deposited on clean glass substrates by thermally evaporating Mn and Bi rods with a purity of 99.99%. During evaporation the vacuum stayed in the range of 10^{-6} mbar *C*-axis orientation of MnBi thin

films could be achieved by adjusting the deposition rates of Mn and Bi to 0.2 and 0.04 nm/s, respectively. After deposition, the Bi/Mn sequences were annealed in a quartz tube in a vacuum of 10^{-5} mbar. All Bi/Mn multilayers were annealed for 1 h, at an annealing temperature depending on the number of Bi/Mn sequences deposited. (Bi/Mn)_x multilayers consisting of one, two, and three Bi/Mn sequences were annealed at 300, 310, and 320 °C, respectively.

The films were characterized by x-ray diffraction analysis (XRD), polarizing microscopy, scanning electron microscopy (SEM), energy-dispersive x-ray analysis (EDX), and SQUID magnetometry. The coercive field, H_c , was determined by polar Kerr hysteresis-loop measurements at a photon energy of 1.8 eV at room temperature. In detail, the preparation and characterization of MnBi thin films were described elsewhere.^{7,8}

III. STRUCTURAL AND MAGNETIC PROPERTIES

X-ray diffraction patterns of the MnBi films show strong MnBi(000*l*) reflections, which indicate NiAs-type structure and full texture with the *c* axis of the crystallites perpendicular to the film plane.⁷ As measured by EDX the Mn to Bi ratio varied in the range of 0.55 to 0.6. The Mn surplus is necessary because part of the Mn is oxidized during the deposition process and during annealing.

In SEM measurements⁷ an enlargement of the MnBi crystallite size was clearly observed when increasing the number of Bi/Mn sequences, i.e., the thickness of the MnBi films. From the SEM pictures the lateral dimension of MnBi crystallites of films consisting of one and three Bi/Mn sequences can be estimated to be smaller than 50 nm and just about 300 nm, respectively. The enlargement of the MnBi crystallites coincides with a decreasing reflectivity from 42% to 5% at a photon energy of 1.8 eV due to increased surface roughness.

The saturation magnetization M_s of the MnBi films is 420 kA/m as determined by SQUID magnetometry. The value of M_s of our films is smaller than the reported bulk value. This discrepancy is probably due to a reduced density of the MnBi films.^{5,6} The coercive field H_c decreases from 1.25 to 0.36 T as the thickness of the MnBi films increases from 41.7 to 90 nm.⁷ In addition, the shape of the polar Kerr hysteresis loops changes. Whereas the 90-nm-thick MnBi film exhibits a steep onset of the magnetization reversal process, the magnetization reversal of the 41.7-nm film starts very slowly. Independent of film thickness, magnetic fields of up to 2.0 T are necessary to saturate the magnetization completely.

IV. A MICROMAGNETIC MODEL

For a theoretical description of the Bi/Mn multilayers the film is assumed to consist of cells on a square lattice with a square base of size L^2 and a height h .⁹ Due to the high anisotropy of the Bi/Mn multilayers the grains are magnetized perpendicular to the film surface with a uniform magnetization M_s of 420 kA/m. The grains interact via domain-wall energy and dipole interaction. The coupling of the magnetization to an external magnetic field H is taken into account as well as an energy barrier which has to be overcome to initiate the reversal process of a single cell.¹⁰⁻¹²

The energy change of the system due to the reversal of a single cell i with magnetization $L^2 h M_s \sigma_i$ and $\sigma_{i,j} = \pm 1$ is

$$\begin{aligned} \Delta E_i &= \Delta E_w + \Delta E_d + \Delta E_H \\ &= -\frac{1}{2} L h S_w \Delta \sigma_i \sum_{\langle j \rangle} \sigma_j + \frac{\mu_0}{4\pi} M_s^2 L h^2 \Delta \sigma_i \sum_j \frac{\sigma_j}{r_{i,j}^3} \\ &\quad - \mu_0 H L^2 h M_s \Delta \sigma_i, \end{aligned} \quad (1)$$

where

$$\Delta \sigma_i = \sigma_i(\text{new}) - \sigma_i(\text{old}) = \pm 2. \quad (2)$$

The first term describes the wall energy change ΔE_w . The sum is over the four next neighbors. S_w should be smaller than the Bloch-wall energy which is $S_B = 0.016 \text{ J/m}^2$ for MnBi,⁶ since the crystalline structure of the system is interrupted at the grain boundary and since, due to the irregular shape, the grains are not connected by the entire surface. The simulation results are in good agreement with experimental data for $S_w = 0.004 \text{ J/m}^2$.

In the second term, describing the change of dipole coupling ΔE_d , the sum is over all cells. Here, $r_{i,j}$ is the distance between two cells i and j in units of the lattice constant L . The dependence of the dipole interaction on the distance $r_{i,j}$ is an approximation for large distances. For smaller distances a corrected form was taken into account numerically.

The third term ΔE_H (Zeeman energy) describes the change of coupling energy to an external field.

Additionally, we introduce an energy barrier δ_i as mentioned above. Two reversal mechanisms can be considered as limiting cases: (i) Coherent rotation of the magnetization vector described by an angle θ . In this case the anisotropy leads to an energy barrier of $L^2 h K_u$ where $K_u = 1160 \text{ kJ/m}^3$ is the uniaxial anisotropy constant.⁵ (ii) Domain-wall motion through the grain: In this case the en-

ergy barrier is the Bloch-wall energy $L h S_B$. Note that for the MnBi system considered the Bloch-wall width $d_w = S_B / K_u = 13.7 \text{ nm}$ is smaller than L , so that the wall fits completely within the grain.¹³ We assume that the orientation of the Bloch wall is perpendicular to the film surface. This is energetically favorable due to the dipole interaction and since the area of the wall is smaller in that case.

Comparing these two energies for Bi/Mn multilayers one finds that domain-wall motion has the lower energy barrier so that in the following only this mechanism will be taken into account. We assume that during the reversal process the energy barrier reaches its maximum value $L h S_B$ when the domain wall is in the center of the cell, i.e., when half of the cell is reversed. Consequently, the energy barrier which is relevant for the reversal process is reduced to $\delta = \max(0, L h S_B - \frac{1}{2}(E_w + E_d + E_H))$.

In order to simulate the Bi/Mn multilayers realistically, disorder in grain size has to be considered as is evident from the SEM pictures.⁷ In the model above this would correspond to a random distribution of L . However, this can hardly be simulated exactly since it modulates the normalized cell distance $r_{i,j}$ of the dipole interaction. Therefore, as a simplified ansatz to simulate the influence of disorder we randomly distribute L in the energy term that describes the coupling to the external field. Here a random fluctuation of L is most relevant, since this term is the only one that scales quadratic with L . In the simulations we use a distribution which is Gaussian with width Δ_C . Note that through this kind of disorder our model is mapped onto a random-field model.

The simulation of the model above was done as in an earlier publication¹² via Monte Carlo methods¹⁴ using the Metropolis algorithm with an additional energy barrier. The algorithm satisfies detailed balance and Glauber dynamics consequently. The size of the lattice was typically 150×150 . The dipole interaction was taken into account rigorously without any cutoff or mean-field approximation. The boundary conditions were open. All simulations are performed for room temperature (300 K). In contrast to earlier simulations on CoPt,¹² the influence of thermal fluctuations seems to be negligible here since the range of energies that is relevant for the flip of a cell is rather large compared to room temperature. However, in the limit of very low temperatures the Monte Carlo algorithm passes into an energy-minimization algorithm with single spin-flip dynamics, which can also be used for the investigation of hysteresis.

In Fig. 1 the simulated hysteresis loops are compared with experimental data using grain sizes which are taken from the experiment. Quantitatively the agreement is reasonable. The relevant fields are smaller in the simulation by a factor 2. Clearly, the model above is too simple to be used for a precise determination of coercive fields. Qualitatively the agreement is very good in the sense that the shapes of the experimental loops are reproduced. A thicker magnetic film has a lower coercive field and a more rectangular shape. Apart from this, the shape of the 90-nm film is clearly asymmetric in the sense that there is a steep descent at the beginning of the hysteresis and a finite slope later with a long tail. The change of the nucleation field H_n and the saturation field H_s can be understood by the change of the geometry of the grains. Imagine a long-range ordered system with positive

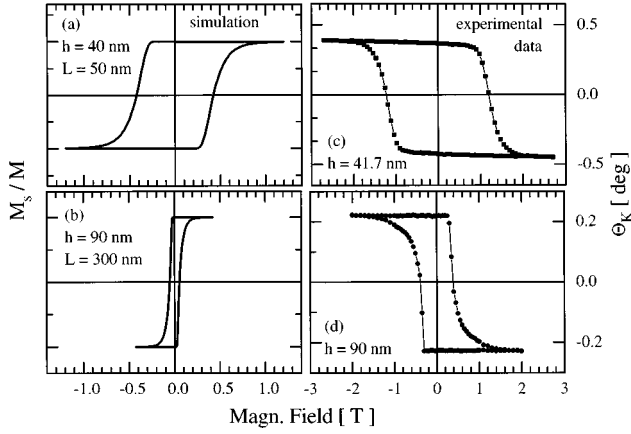


FIG. 1. Calculated hysteresis loops for two grain sizes (a) $h=40$ nm, $L=50$ nm, and (b) $h=90$ nm, $L=300$ nm as compared to experimental data with film thickness (c) $h=41.7$ nm and (d) 90 nm.

magnetization in a negative external field. The first grain reverses its magnetization when the driving forces, i.e., the external field plus the dipole field are large enough to overcome the energy barrier plus the domain-wall energy, i.e.,

$$2\mu_0|H_n|L^2hM_s + \frac{\mu_0}{2\pi}M_s^2Lh^2\sum_j \frac{1}{r_{i,j}^3} > 4LhS_w + \delta. \quad (3)$$

From this ‘‘rule of thumb,’’ which of course neglects the influence of disorder as well as thermal fluctuations, it follows directly that the larger the grain size the smaller is the nucleation field. A similar consideration for the last grain that flips, i.e., the saturation field, leads to

$$2\mu_0|H_s|L^2hM_s - \frac{\mu_0}{2\pi}M_s^2Lh^2\sum_j \frac{1}{r_{i,j}^3} > -4LhS_w + \delta, \quad (4)$$

i.e.,

$$|H_s| - |H_n| = \frac{M_s h}{2\pi L} \sum_j \frac{1}{r_{i,j}^3} - \frac{4S_w}{\mu_0 M_s L}. \quad (5)$$

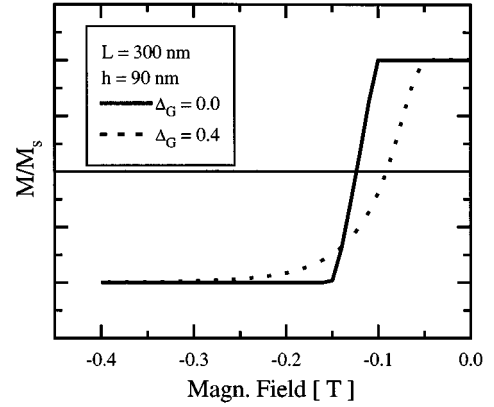


FIG. 2. Disorder dependence of the hysteresis loops for $h=90$ nm and $L=300$ nm using a Gaussian distribution having a width $\Delta_G=0.0$ (solid line) and $\Delta_G=0.4$ (dotted line).

This explains that the width of the loop decreases when the diameter L of the grains increases more rapidly than the thickness h of the film. Note that this is contrary to a former publication on CoPt films where L was constant and h changed.¹² In the latter case a rectangular loop, i.e., $|H_s| - |H_n| = 0$, is obtained for h small enough.

The asymmetry of the hysteresis loops stems from disorder. This is shown in Fig. 2, where the disorder dependence of the hysteresis loop for the case of the 90-nm-thick film is shown. Without disorder ($\Delta_G=0.0$) the loop is symmetric. Through the disorder [$\Delta_G=0.4$ as in Figs. 1(a) and 1(b)] the loop becomes asymmetric. At least one reason for this effect can be understood easily: From Eq. (3) it follows that in the presence of fluctuations of the grain size L the largest grains are the first that reverse their magnetization. For these grains having a large magnetization, the change of magnetization, i.e., the slope of the hysteresis curve, is largest at the beginning of the magnetization reversal.

ACKNOWLEDGMENTS

This work was supported by the German Federal Ministry for Education and Research ‘‘BMBF’’ under Grant No. FKZ 13N6178/2.

¹D. Chen, J. Appl. Phys. **37**, 1486 (1966).

²H. J. Williams, R. C. Sherwood, F. G. Foster, and E. M. Kelly, J. Appl. Phys. **28**, 1181 (1957).

³L. Mayer, J. Appl. Phys. **31**, 384S (1960).

⁴Y. J. Wang, J. Magn. Magn. Mater. **84**, 39 (1990).

⁵T. Chen and W. E. Stutius, IEEE Trans. Magn. **MAG-10**, 581 (1974).

⁶X. Guo, X. Chen, Z. Altounian, and J. O. Ström-Olsen, J. Appl. Phys. **73**, 6275 (1993).

⁷U. Rüdiger, H. Berndt, A. Schirmeisen, P. Fumagalli, and G. Güntherodt, J. Appl. Phys. **78**, 5391 (1995).

⁸U. Rüdiger, P. Fumagalli, H. Berndt, A. Schirmeisen, and G.

Güntherodt, J. Appl. Phys. **80**, 196 (1996).

⁹W. Andrä, H. Danan, and R. Mattheis, Phys. Status Solidi A **125**, 9 (1991).

¹⁰R. D. Kirby, J. X. Shen, R. J. Hardy, and D. J. Sellmyer, Phys. Rev. B **49**, 10 810 (1994).

¹¹T. Kleinfeld, J. Valentin, and D. Weller, J. Magn. Magn. Mater. **148**, 249 (1994).

¹²U. Nowak, IEEE Trans. Mag. **31**, 4169 (1995).

¹³C. Kittel, Phys. Rev. **73**, 810 (1948).

¹⁴K. Binder, *Monte Carlo Methods in Statistical Physics* (Springer, Berlin, 1979).